Supporting Information

Amplification Effect of Side Groups Regulation via Imidazolate linkages of Covalent Organic Frameworks for Efficient Oxygen Reduction

Mengyuan Chen,[a,b] Zhiqiang Zhu,[b] Youxin Ji,[a]* Xiangtao Kong,[c] Diandian Han,[b]* and Lipeng Zhai[b]*

[a] National Engineering Research Center for Advanced Polymer Processing Technology, The Key Laboratory of Material Processing and Mold of Ministry of Education, College of Materials Science and Engineering, Zhengzhou University, Zhengzhou, 450002, P. R. China

[b] Department Henan Key Laboratory of Functional Salt Materials, Center for Advanced Materials Research, Zhongyuan University of Technology, Zhengzhou 450007, P. R. China

[c] Henan Key Laboratory of New Optoelectronic Functional Materials, College of Chemistry and Chemical Engineering, Anyang Normal University, Anyang 455000, P. R. China [a] Center for Advanced Materials Research, Zhongyuan University of Technology, Henan 450007, P. R. China

* Corresponding author. E-mail address: *yxji@zzu.edu.cn, 6788@zut.edu.cn, zhailp@zut.edu.cn.*

Contents

Section 1. Methods and Materials

Methods. Characterization. Fourier transform infrared (FT-IR) spectra were measured on a Nicolet iS50 FT-IR. Powder X-ray diffraction (PXRD) data were performed on a Bruker D8 Focus Powder X-ray Diffractometer by using powder on glass substrate, from 2θ = 2° up to 30° with 0.01° increment. Morphology images were obtained on a Zeiss Merlin Compact filed emission scanning electron microscope (FE-SEM) equipped with an energy dispersive X-ray spectroscopy (EDS) system at an electric voltage of 5 KV. TEM and high-resolution TEM (HRTEM) images were obtained using a JEOL JEM-F200 with an accelerating voltage of 200 kV. The Brunauer-Emmett-Teller (BET) method was utilized to calculate the specific surface areas. By using the N_2 adsorption-desorption isotherms were collected on a TriStar II instrument (Micromeritics) at 77K to calculate the specific surface areas. The nonlocal density functional theory (NLDFT) model was used to estimate pore size distribution by adsorption isotherm. Ultraviolet-visible absorption spectra were investigated on an Agilent Cary 100 UV/Vis spectrophotometer with background correction. Thermogravimetric analysis (TGA) was recorded on a Mettler TGA/DSC 3^+ in N_2 atmosphere from 30 °C to 800 °C at the rate of 10 °C min-1. Solid-state ^{13}C NMR (100 MHz or 150 MHz) spectral data were carried out with Bruker Avance spectrometers, where chemical shifts (δ in ppm) were determined with a residual proton of the solvent as standard.

Materials. 2,7-ditert-butylpyrene-4,5,8,10-tetraone was purchased from Zhengzhou Alpha Chemical Co., Ltd. Ammonium acetate was purchased from Anhui Senrise Technology Co.,Ltd. 1,3,5-tris(4-formylphenyl) benzene and 1,3,5-tris(3-fluoro-4-formylphenyl) benzene were purchased from Jilin Zhongkeshen Technology Co., Ltd. 5'-(4-formyl-3-methoxyphenyl)-3,3''-dimethoxy-[1,1':3',1''-terphenyl]-4,4''-dicarbaldehyde and 5'-(4-formyl-3-hydroxyphenyl)-3,3''-dihydroxy-[1,1':3',1''-terphenyl]-4,4''-dicarbaldehyde were purchased from Henan Pusai Chemical Products Co., Ltd. 1,2-Dichlorobenzene (o-DCB), mesitylene, ethanol, n-butanol (n-BuOH), and Tetrahydrofuran (THF) were purchased from energychemical. All the other solvents were purchased from Aladdin Chemicals and used as received without further purification.

Synthesis of H-COF: 2,7-ditert-butylpyrene-4,5,8,10-tetraone (17 mg, 0.045 mmol), ammonium acetate (21 mg, 0.270 mmol), and 1,3,5-tris(4-formylphenyl) benzene (12 mg, 0.030 mmol) were weighed into a Pyrex tube (10 mL). To the mixture was added dioxane (0.2 mL) and mesitylene (0.8 mL). The mixture was then sonicated for 1 min until they were completely dissolved and then the solution was degassed by three freeze-pump-thaw cycles. The tube was flame sealed and placed in an oven at 150 °C for 5 days after warming to room temperature, yielding a yellow green solid. The solid was isolated by centrifugation and washed with ethanol and THF for three times and then purified by Soxhlet extraction with THF as the solvent for 48 hours. The powder was collected and dried at 80 °C under vacuum overnight to yield H-COF as yellow green powder (81% yield).

Synthesis of F-COF: 2,7-ditert-butylpyrene-4,5,8,10-tetraone (17 mg, 0.045 mmol), ammonium acetate (21 mg, 0.270 mmol), and 1,3,5-tris(3-fluoro-4-formylphenyl) benzene (14 mg, 0.030 mmol) were weighed into a Pyrex tube (10 mL). To the mixture was added dioxane (0.5 mL) and mesitylene (0.5 mL). The mixture was then sonicated for 1 min until they were completely dissolved and then the solution was degassed by three freeze-pump-thaw cycles. The tube was flame sealed and placed in an oven at 150 °C for 5 days after warming to room temperature, yielding a light brown solid. The solid was isolated by centrifugation and washed with ethanol and THF for three times and then purified by Soxhlet extraction with THF as the solvent for 48 hours. The powder was collected and dried at 80 °C under vacuum overnight to yield F-COF as light brown powder (80% yield).

Synthesis of OMe-COF: 2,7-ditert-butylpyrene-4,5,8,10-tetraone (17.6 mg, 0.0465 mmol), ammonium acetate (21.7 mg, 0.279 mmol), and 5'-(4-formyl-3-methoxyphenyl)-3,3''-dimethoxy-[1,1':3',1''-terphenyl]-4,4''-dicarbaldehyde (15 mg, 0.031 mmol) were weighed into a Pyrex tube (10 mL). To the mixture was added dioxane (0.5 mL) and mesitylene (0.5 mL). The mixture was then sonicated for 1 min until they were completely dissolved and then the solution was degassed by three freeze-pump-thaw cycles. The tube was flame sealed and placed in an oven at 150 °C for 5 days after warming to room temperature, yielding a yellow green solid. The solid was isolated by centrifugation and washed with ethanol and THF for three times and then purified by Soxhlet extraction with THF as the solvent for 48 hours. The powder was collected and dried at 80 °C under vacuum overnight to yield OMe-COF as yellow green powder (85% yield).

Synthesis of OH-COF: 2,7-ditert-butylpyrene-4,5,8,10-tetraone (18 mg, 0.048 mmol), ammonium acetate (22 mg, 0.288 mmol), and 5'-(4-formyl-3-hydroxyphenyl)-3,3''-dihydroxy-[1,1':3',1''-terphenyl]-4,4''-dicarbaldehyde (14 mg, 0.032 mmol) were weighed into a Pyrex tube (10 mL). To the mixture was added dioxane (0.5 mL) and mesitylene (0.5 mL). The mixture was then sonicated for 1 min until they were completely dissolved and then the solution was degassed by three freeze-pump-thaw cycles. The tube was flame sealed and placed in an oven at 150 °C for 5 days upon warming to room temperature, yielding an orange solid. The solid was isolated by centrifugation and washed with ethanol and THF for three times and then purified by Soxhlet extraction with THF as the solvent for 48 hours. The powder was collected and dried at 80 °C under vacuum overnight to yield OH-COF as orange powder (84% yield).

Synthesis of PDA-OMe-COF: p-phenylenediamine (6.49 mg, 0.06 mmol) and 5'-(4-formyl-3-methoxyphenyl)-3,3''-dimethoxy-[1,1':3',1''-terphenyl]-4,4''-dicarbaldehyde (19.22 mg, 0.04 mmol) were weighed into a Pyrex tube (10 mL). To the mixture was added dioxane (0.5 mL) and mesitylene (0.5 mL). The mixture was then sonicated for 1 min until they were completely dissolved and added 6 M acetic acid (0.1 mL) to the mixture. Then the solution was degassed by three freeze-pump-thaw cycles. The tube was flame sealed and placed in an oven at 120 °C for 3 days upon warming to room temperature, yielding

an orange yellow solid. The solid was isolated by centrifugation and washed with ethanol and THF for three times and then purified by Soxhlet extraction with THF as the solvent for 48 hours. The powder was collected and dried at 80 °C under vacuum overnight to yield PDA-OMe-COF as orange yellow powder (80% yield).

Computational calculations. The molecular structures were optimized at the TPSS/6-31G* level with Grimme's dispersion correction at the Becke-Johnson damping (D3BJ) level by the ORCA program[S1-S3]. While, the periodic calculations were performed by using the CP2K[S4]. The PBE functional along with Grimme's dispersion correction at the Becke-Johnson damping (D3BJ) level was used for structural optimization[S5]. The wave functions are expanded in a double zeta Gaussian basis set, while the electron density is expanded in Gaussians and auxiliary plane waves (GPW) with an energy cut-off at 400 Rydberg for the electron density. The frequency analyses were carried out at the same level. The single point energies were calculated at the PBE level with a triple-ζ polarization quality Gaussian basis set (TZVP-MOLOPT-GTH). The thermal correction to Gibbs free energies were computed by the Shermo code[S6]. The CP2K input files were created by the Multiwfn package[S7], and the electrostatic potential colored molecular surface were also calculated by the Multiwfn software.

The overall ORR in an alkaline environment is:

$$O_2 + 2H_2O + 4e^- \rightarrow 4OH^-$$

The reaction is divided into four elementary steps:

$$O_2 + H_2O + e^- + * \rightarrow OOH^* + OH^- \quad (1)$$

$$OOH^* + e^- \rightarrow O^* + OH^- \quad (2)$$

$$O^* + H_2O + e^- \rightarrow OH^* + OH^- \quad (3)$$

$$OH^* + e^- \rightarrow OH^- + * \quad (4)$$

in which * implies the adsorption site, and OOH^*, O^* and OH^* are adsorbed intermediates.

For each step, the reaction free energy ΔG_1, ΔG_2, ΔG_3 and ΔG_4 is defined by the following equation:

$$\Delta G = \Delta E_{DFT} + \Delta ZPE - T\Delta S + neU$$

The ΔE_{DFT}, ΔZPE, ΔS and neU are total energy change of the system, zero-point energy variation, entropy change of the reaction and contribution of electrode potential, respectively. The ΔE_{DFT} is calculated by Density functional theory (DFT). The ΔZPE, and ΔS are obtained from the values in ref. S5 and S6. n, e and U are the number of participating electrons, the charge of a single electron (1.602×10^{-19} C) and electrode potential measured at standard conditions (relative to RHE, Reversible Hydrogen Electrode).

The total free energy change (ΔE_{total}) for ORR is obtained by the following equation:

$$\Delta E_{total} = -4.92 \text{ eV} + 4 \text{ eU}$$

-4.92 eV is the total free energy change of O_2 reduction to OH^- under standard conditions (298 K, 1 atm).

Electrocatalytic measurements. The electrochemical measurements were conducted on a conventional three-electrode cell including glassy carbon electrode as working electrode, Ag/AgCl (3M KCl) as reference electrode and platinum wire as electrode, using the PINE electrochemical workstation (Pine Research Instrumentation, USA) at room temperature. The rotating disk electrode (RDE) tests of prepared four COF catalysts were measured in 0.1 M KOH solution. The ink of catalyst was prepared by mixing 5 mg of catalyst powder and 5 mg multi-walled carbon nanotubes-COOH functionalization with 950 μl of ethanol, 30 μl of isopropanol, 20 μl of Nafion (5 wt%) solution, and further sonicated for 1 h to yield a homogeneous ink. Loading 15 ul ink on the glassy carbon electrode (d=5.00 mm, S=0.19625 cm^2) for ORR performance tests. Linear sweep voltammetry (LSV) was performed in N_2-saturated and O_2-saturated 0.1 M KOH at a scan rate of 10 mV s^{-1} under various electrode rotation rates (400, 625, 900, 1225, and 1600 rpm, respectively). For the cyclic voltammetry (CV) test, the potential range was circularly scanned between -0.80 and 0.10 V at a scan rate of 50 mV s^{-1} after purging O_2 for 30 min. The double layer capacitance was the voltammetry curve measured in N_2-saturated 0.1 M KOH solution. Long-term stability test was conducted at a fixed potential of 0.7 V (vs RHE) at a rotation speed of 1600 rpm in O_2-saturated electrolyte on a CHI 760 E electrochemical workstation by measuring the current changes of the catalyst. Methanol tolerance test was performed by chronoamperometric measurement at 0.7 V (vs RHE) at a rotating speed of 1600 rpm (methanol was dropped into the electrolytes at 200 s).

The rotating ring disk electrode (RRDE) electrode with a Pt ring and a glassy carbon disk served as the substrate for the working electrode for evaluating the ORR activity and selectivity of various catalysts. The RRDE measurements were conducted at a rotation rate of 1600 rpm with a sweep rate of 10 mV s^{-1}. On the basis of ring and disk currents, the electron-transfer number (n) and H_2O_2 yield [H_2O_2 (%)] were calculated from the equations:

$$n = \frac{4 \times |I_d|}{|I_d| + I_r/N}$$

$$H_2O_2(\%) = \frac{2I_r/N}{|I_d| + I_r/N} \times 100\%$$

where I_d is the disk current, I_r is the ring currents, and N is the ring collection efficiency (N=37%).

The current density was normalized to the geometrical area and the measured potentials vs. Ag/AgCl were converted to a reversible hydrogen electrode (RHE) scale according to the following equation:

$$E_{RHE} = E_{Ag/AgCl} + 0.1976 + 0.059 * pH$$

The Tafel slope was estimated by linear fitting of the polarization curves according to following equation:

$$\eta = a + b * log|j|$$

where j is the current density and b is the Tafel slope.

The turnover frequency (TOF) was evaluated by the following equation:

$$TOF = \frac{J \times A}{4 \times F \times n}$$

where J (A cm^{-2}) is the current density at a given potential (0.7 V), A is the surface area of the electrode (0.19625 cm2), F stands for the Faraday constant (96500 C mol^{-1}), the number of 4 represents 4 electrons mol^{-1} of O_2, and n stands for the number of moles of C atoms in samples.

The mass activity value is calculated according to the following equation:

$$Mass\ Activity = \frac{J \times A}{m}$$

Where J is the current density at a given potential (0.7 V), A is the surface area of the electrode (0.19625 cm^2) and m is the sample mass loaded on electrode.

Zn-air battery test. The air electrodes were prepared by uniformly coating the as-prepared catalyst ink onto carbon paper and then drying it at 100 °C for 2 h with 1.0 mg cm^{-2} mass loading, and the Zinc plate was used as the anode. Both electrodes were assembled into a home-built electrochemical battery with 6 M KOH + 0.2 M $Zn(CH_3COO)_2 \cdot 2H_2O$ electrolyte. The discharge polarization curve measurements were performed at 10 mV s^{-1} on a CHI660 electrochemical workstation at room temperature. The galvanostatic discharge curve was tested on a LAND testing system.

Section 2. Supporting Figures

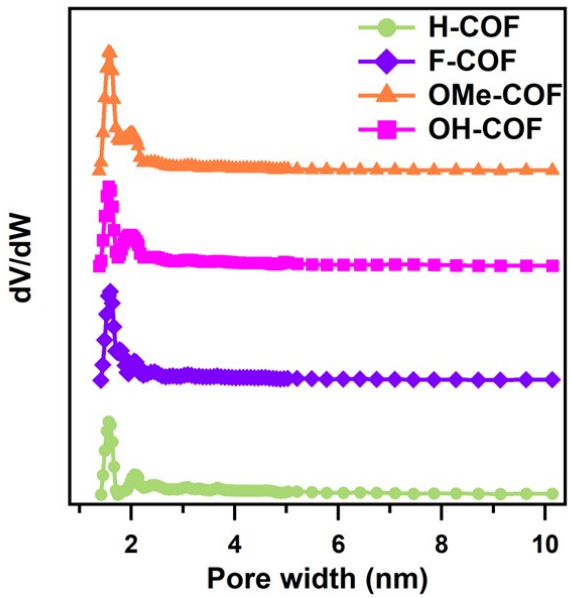

Figure S1. Pore size distribution of H-COF, F-COF, OMe-COF, and OH-COF.

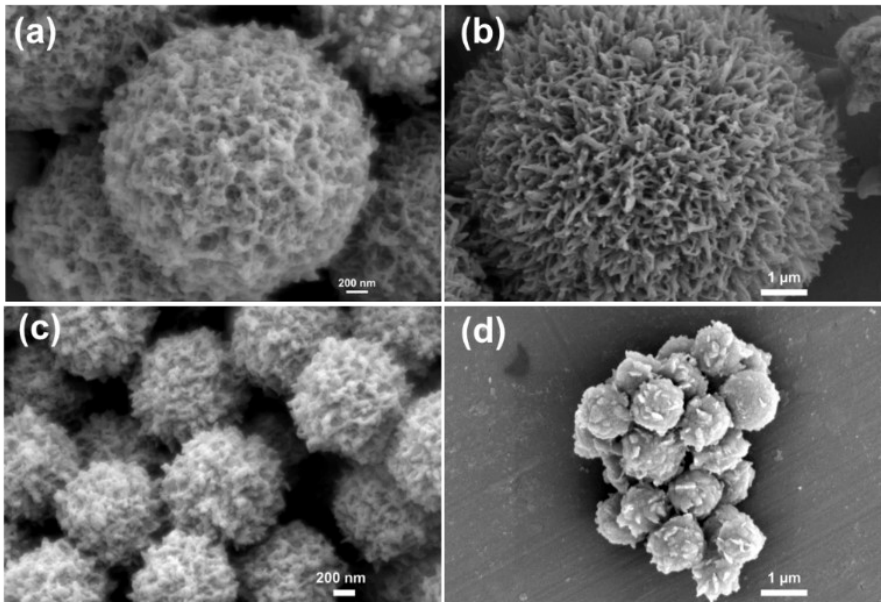

Figure S2. SEM images of (a) H-COF, (b) F-COF, (c) OMe-COF and (d) OH-COF.

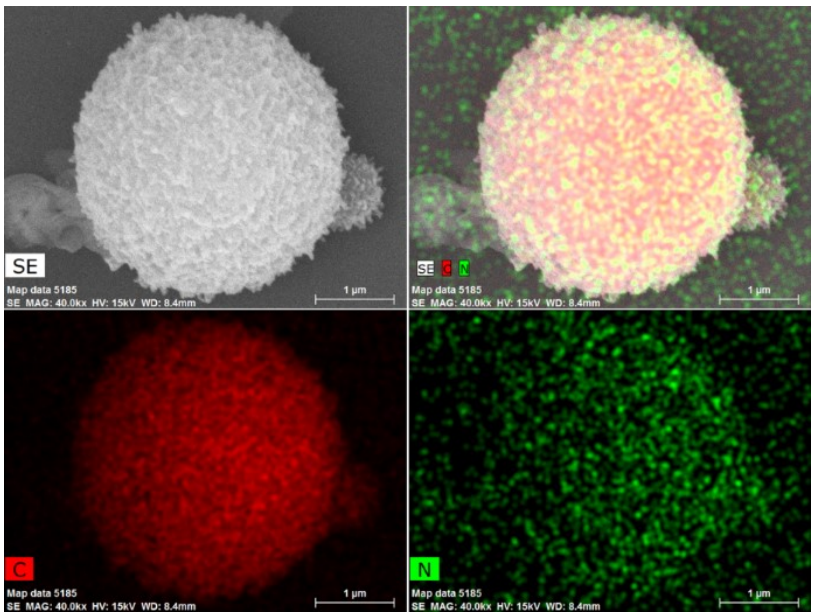

Figure S3. The EDS mapping images of H-COF.

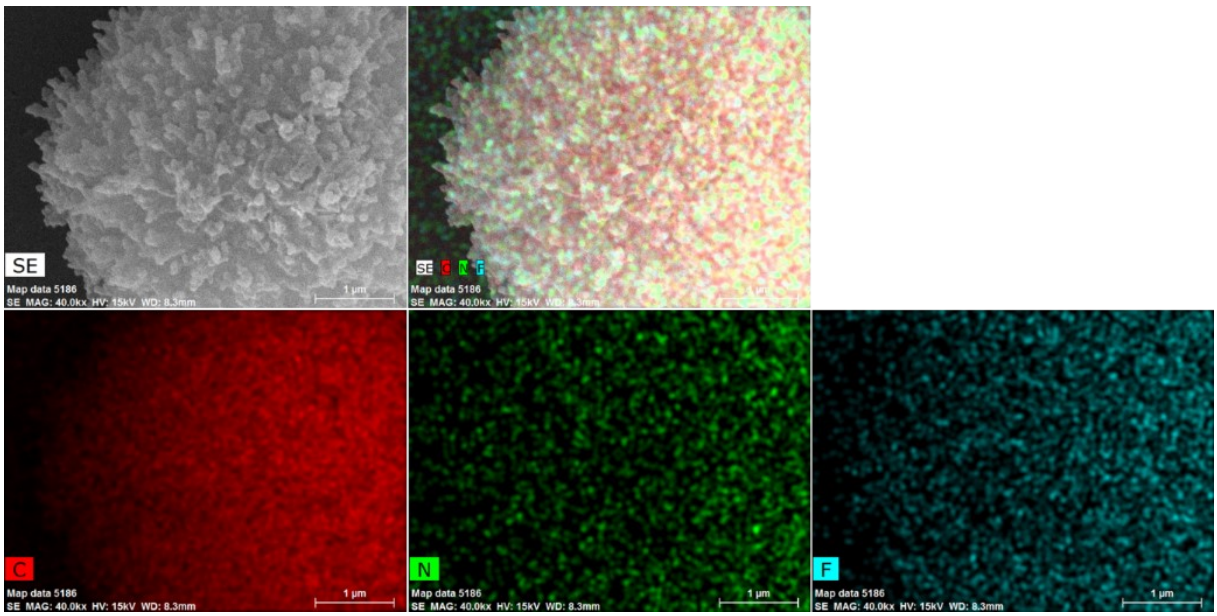

Figure S4. The EDS mapping images of F-COF.

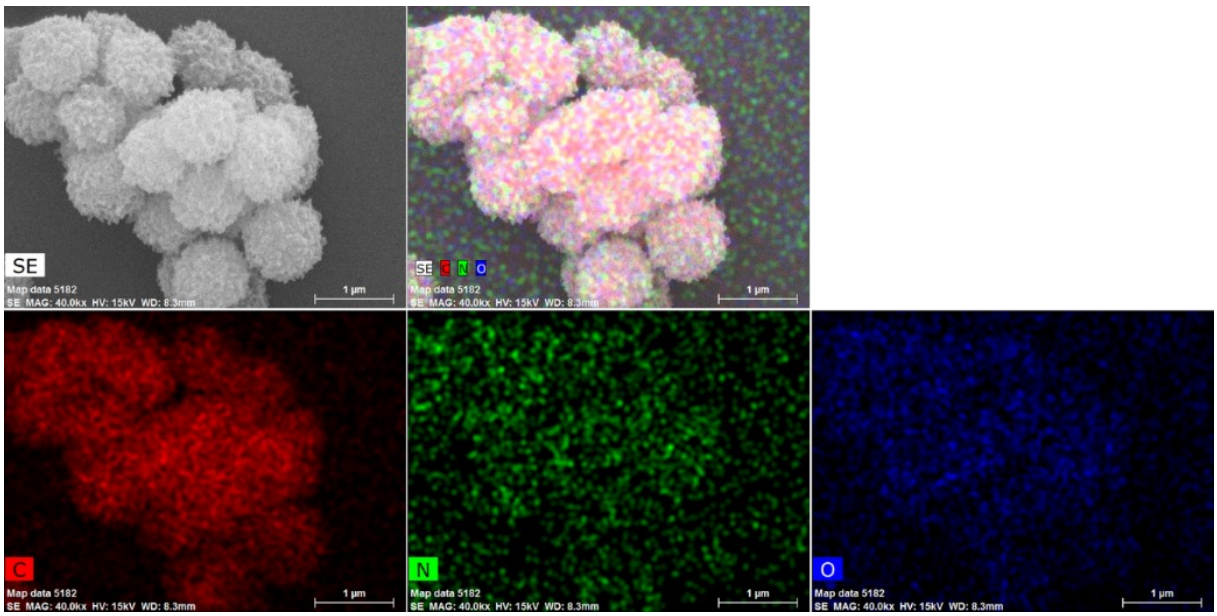

Figure S5. The EDS mapping images of OMe-COF.

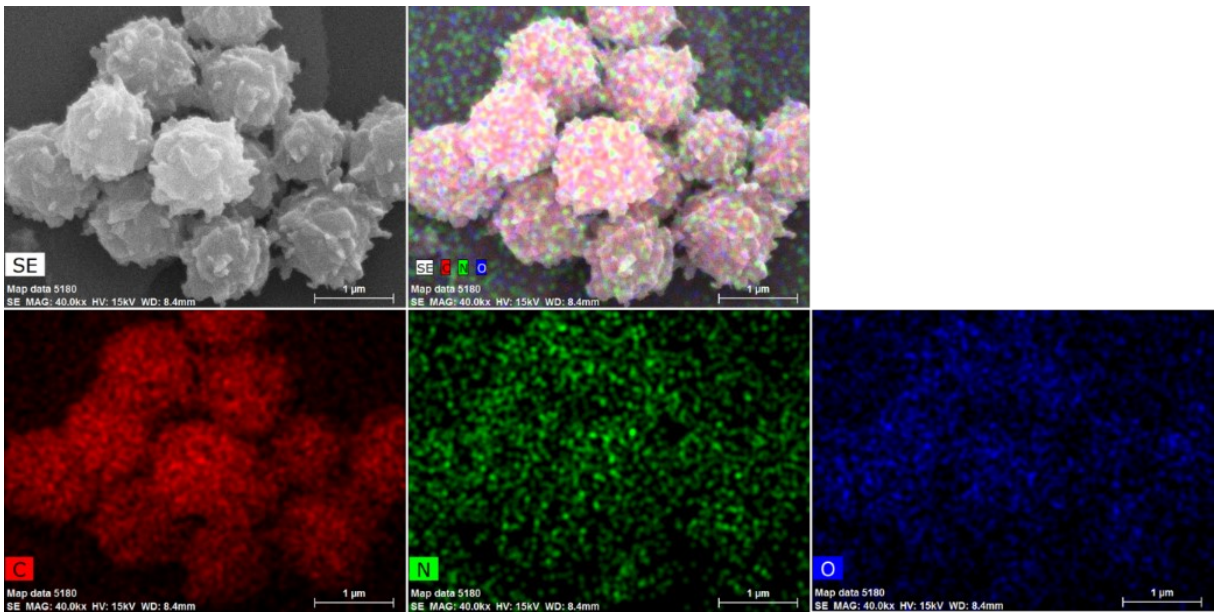

Figure S6. The EDS mapping images of OH-COF.

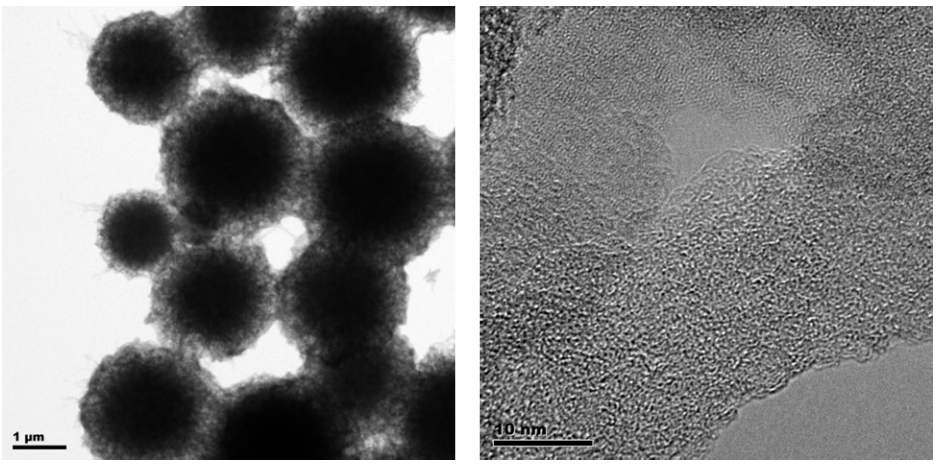

Figure S7. TEM images of H-COF.

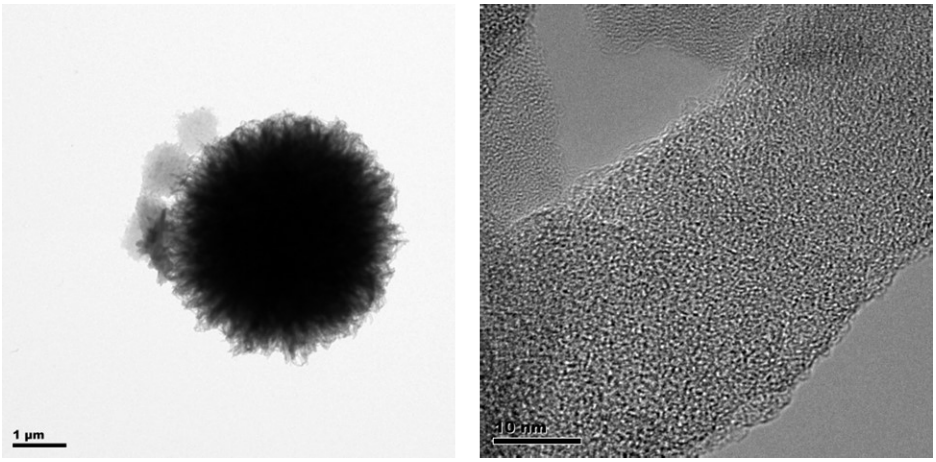

Figure S8. TEM images of F-COF.

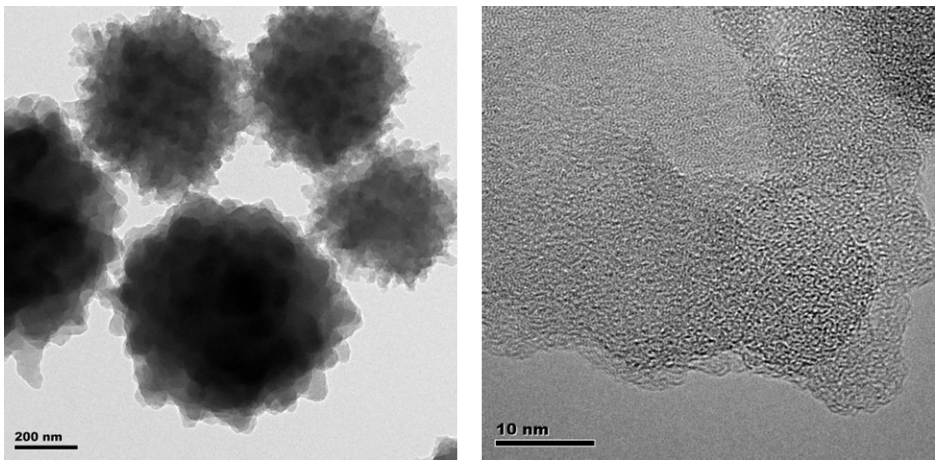

Figure S9. TEM images of OMe-COF.

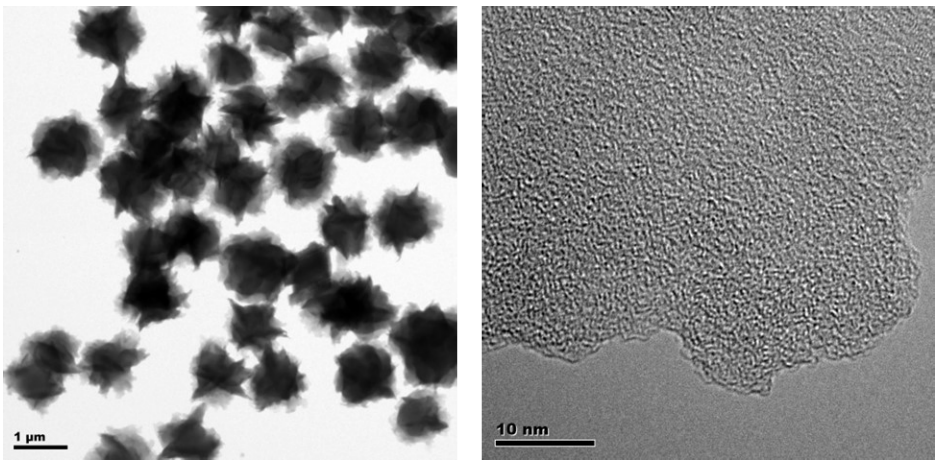

Figure S10. TEM images of OH-COF.

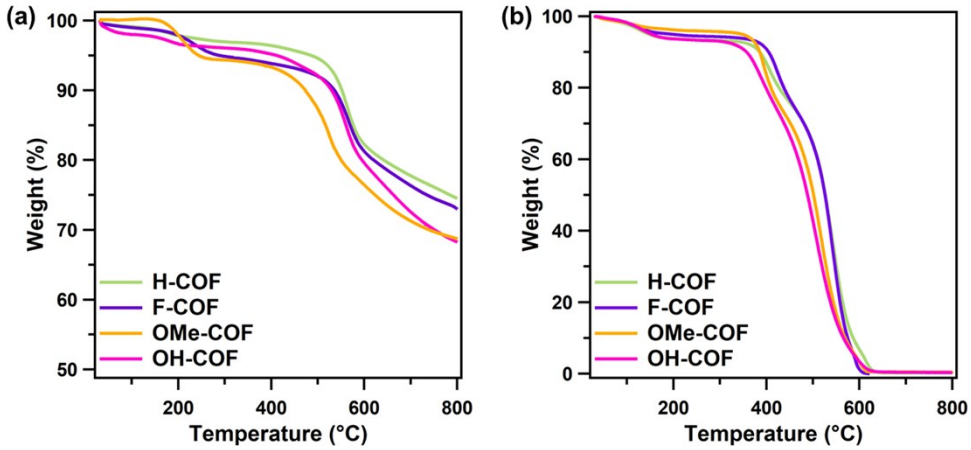

Figure S11. TGA curves of H-COF, F-COF, OMe-COF and OH-COF in (a) N_2 and (b) air.

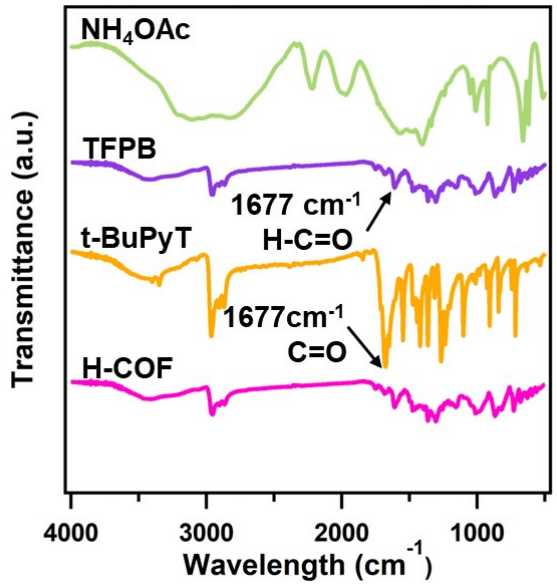

Figure S12. FT-IR spectra of NH_4OAc, TFPB, t-BuPyT and H-COF.

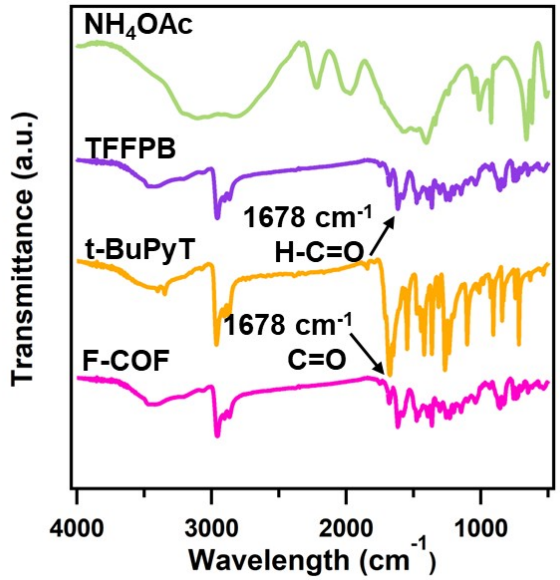

Figure S13. FT-IR spectra of NH_4OAc, TFFPB, t-BuPyT and F-COF.

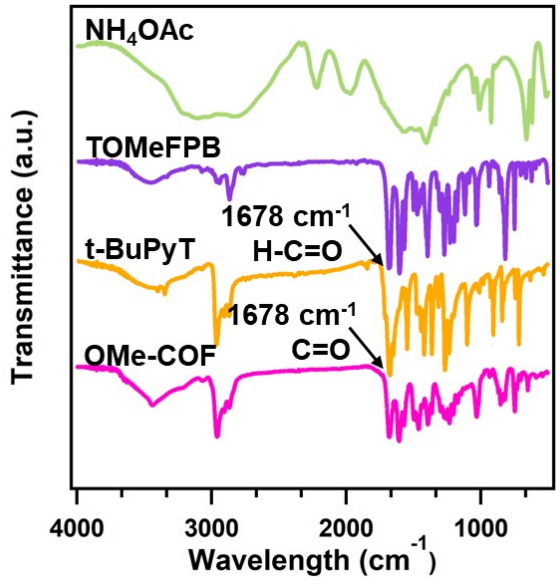

Figure S14. FT-IR spectra of NH_4OAc, TOMeFPB, t-BuPyT and OMe-COF.

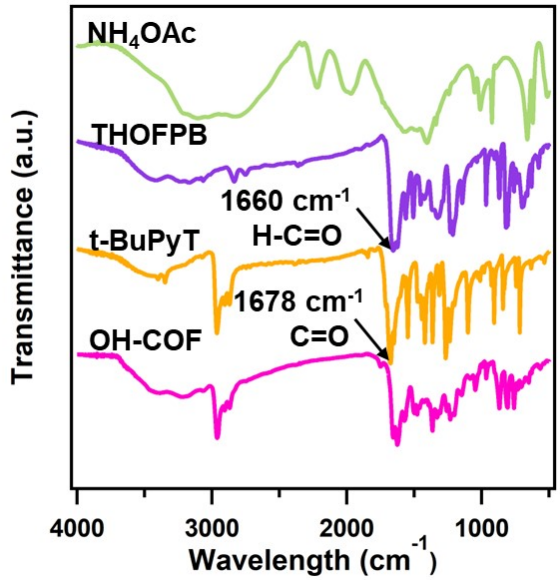

Figure S15. FT-IR spectra of NH_4OAc, TFFPB, t-BuPyT and OH-COF.

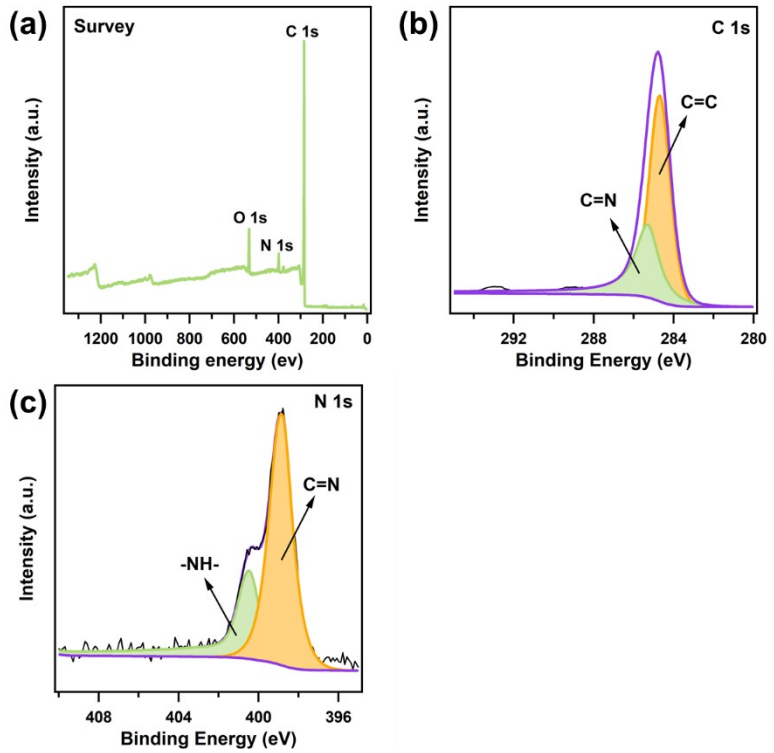

Figure S16. XPS spectra for (a) Survey, (b) C 1s, (c) N 1s of H-COF.

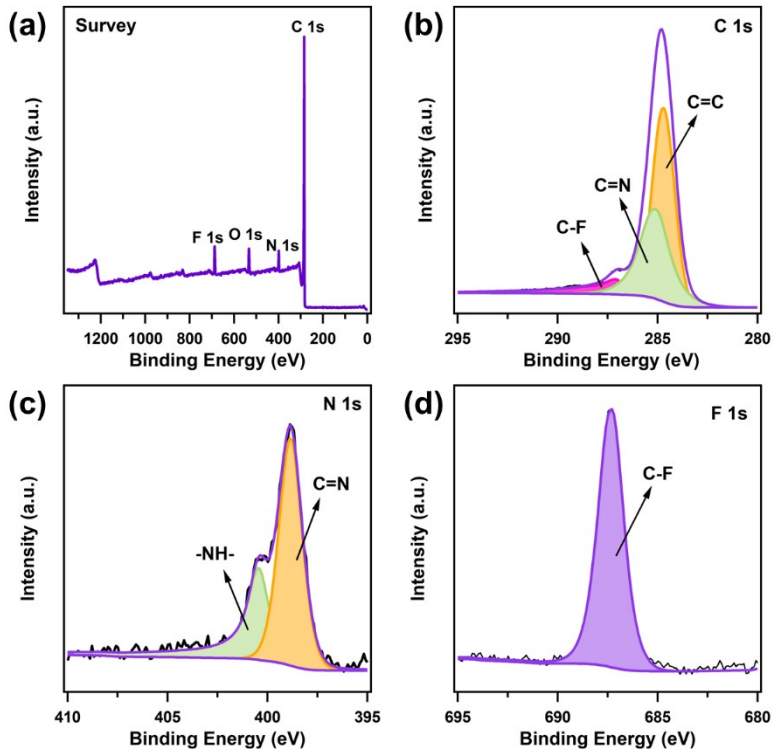

Figure S17. XPS spectra for (a) Survey, (b) C 1s, (c) N 1s and (d) F 1s of F-COF.

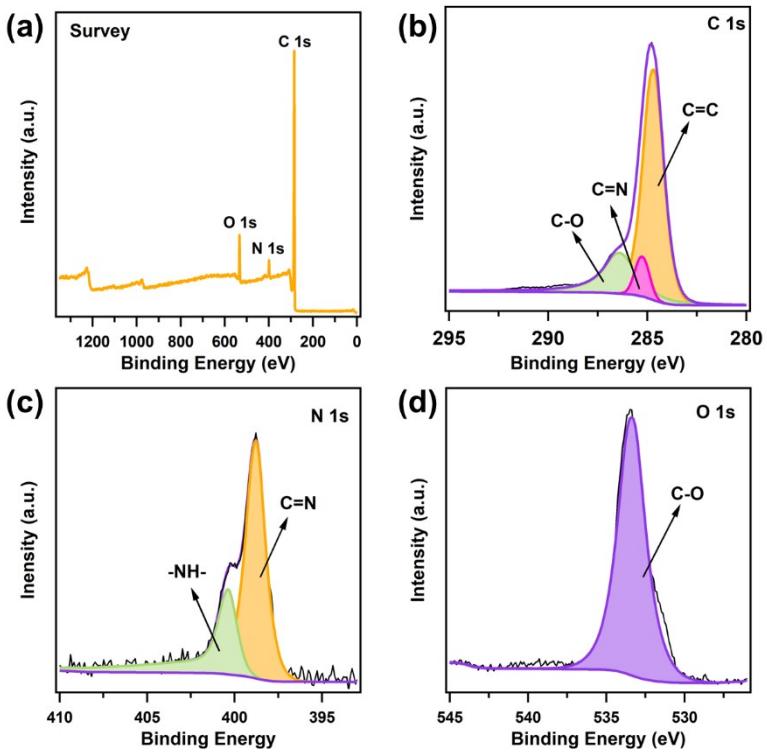

Figure S18. XPS spectra for (a) Survey, (b) C 1s, (c) N 1s and (d) O 1s of OMe-COF.

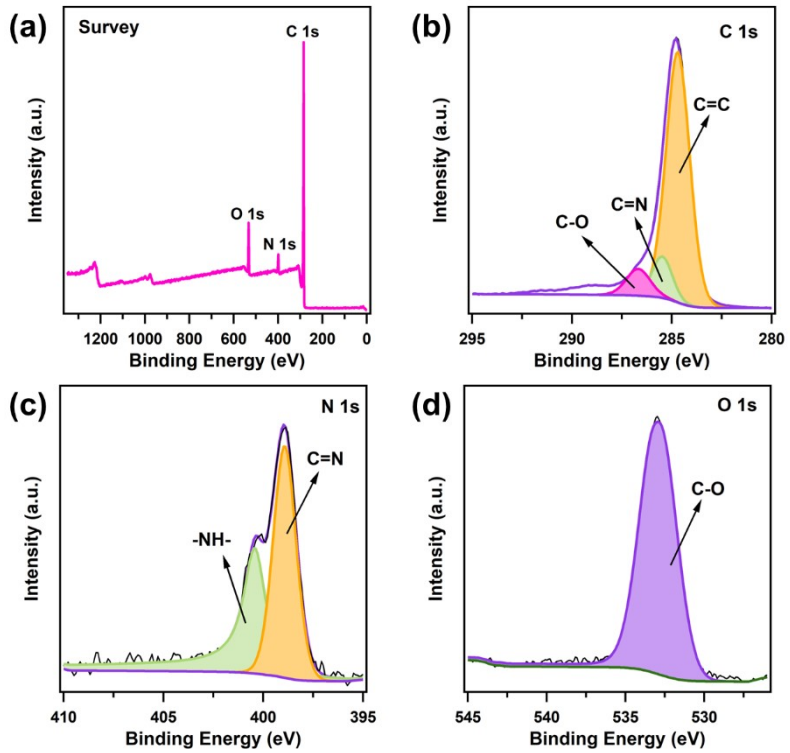

Figure S19. XPS spectra for (a) Survey, (b) C 1s, (c) N 1s and (d) O 1s of OH-COF.

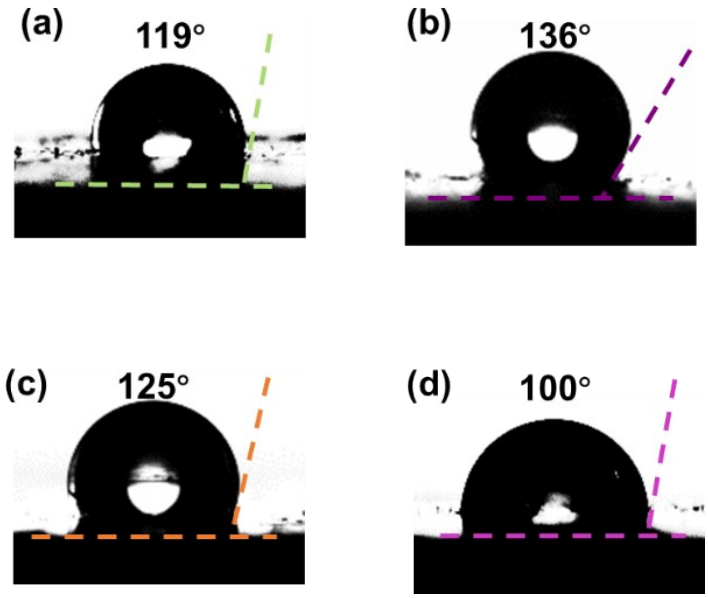

Figure S20. Images of contact angle measurements of (a) H-COF, (b) F-COF, (c) OMe-COF, and (d) OH-COF.

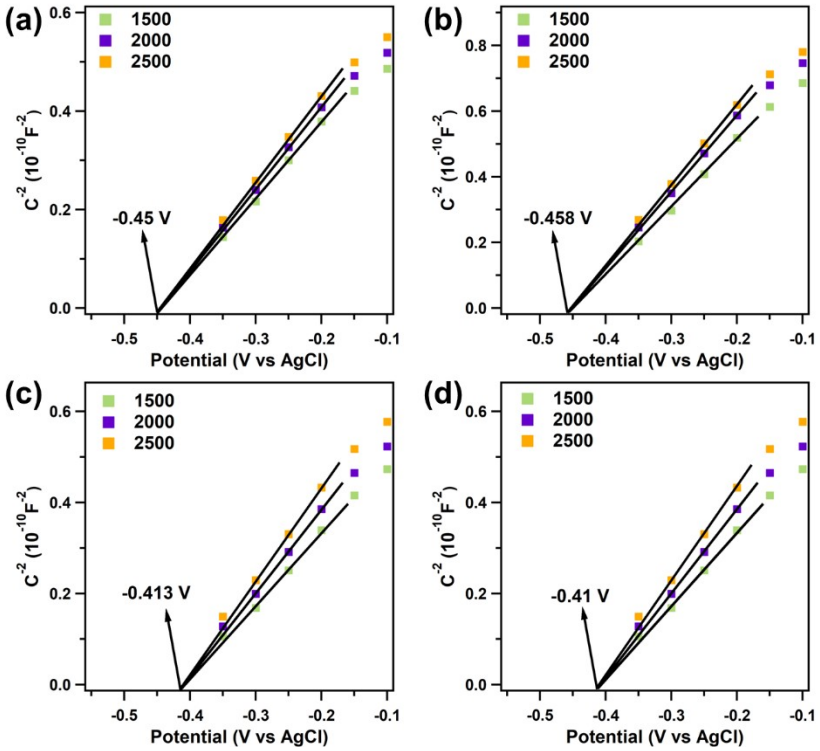

Figure S21. Mott-Schottky plots of (a) H-COF, (b) F-COF, (c) OMe-COF and (d) OH-COF (in 0.5 M Na_2SO_4, scan rate 10 mV s^{-1}).

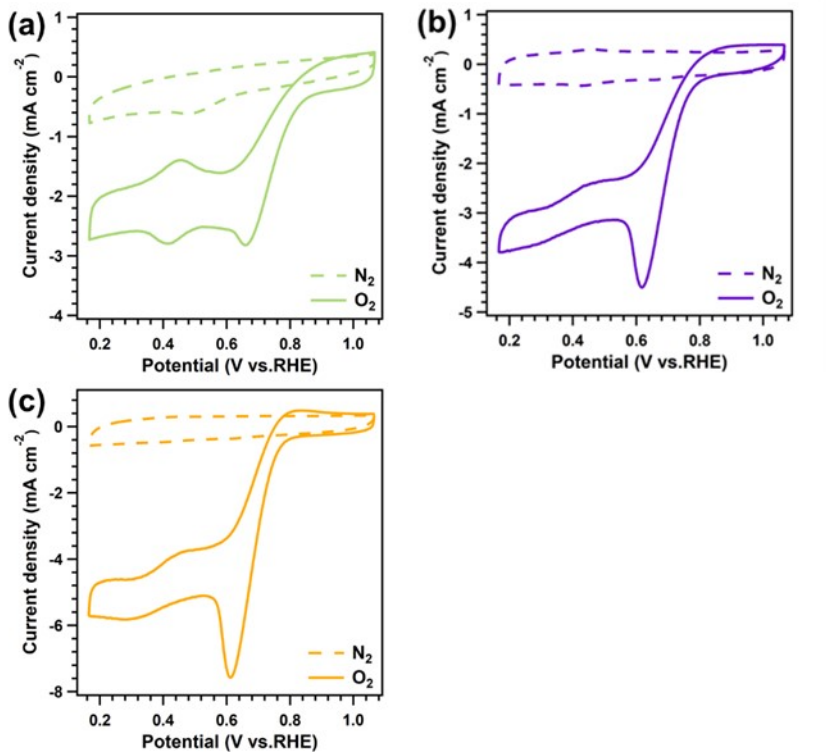

Figure S22. CV curves for (a) H-COF, (b) F-COF, (c) OMe-COF and (d) OH-COF in O_2-saturated (solid curve) and N_2-saturated (dotted curve).

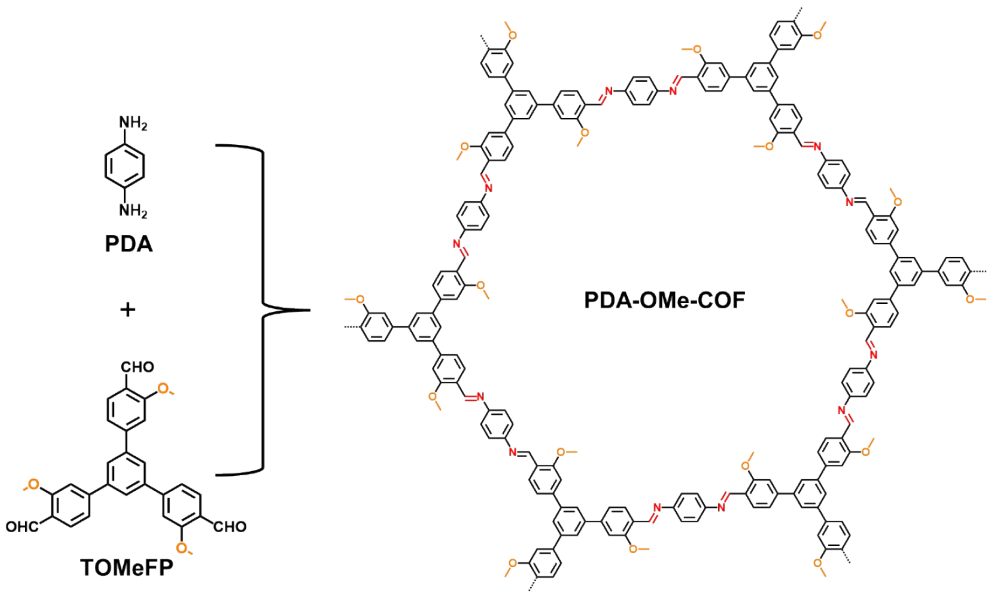

Figure S23. Synthesis and structure of PDA-OMe-COF.

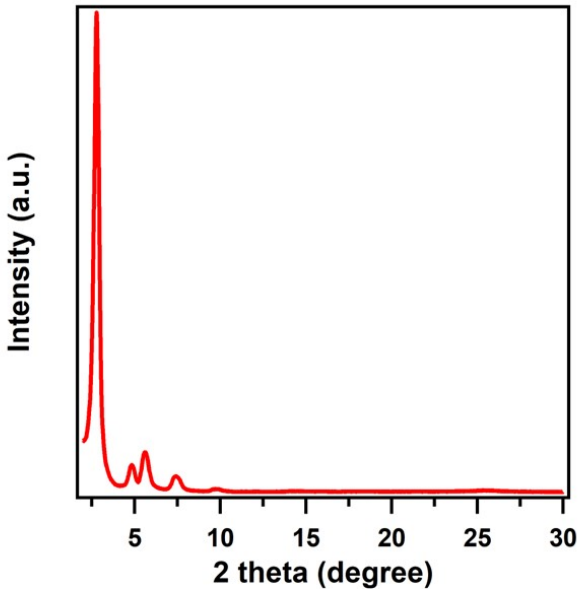

Figure S24. PXRD of PDA-OMe-COF.

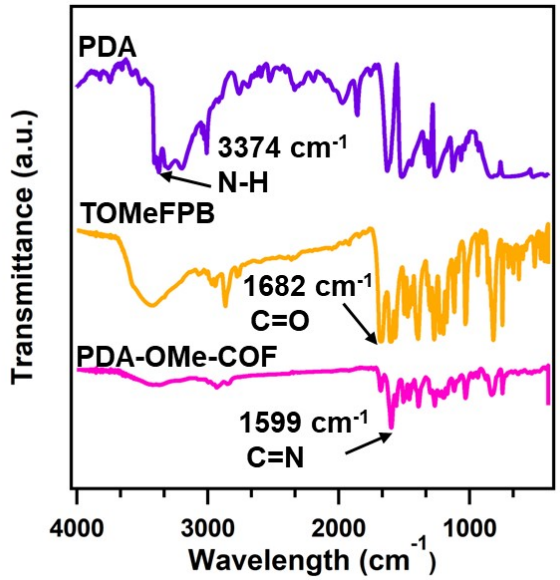

Figure S25. FT-IR spectra of PDA, TOMeFPB and PDA-OMe-COF.

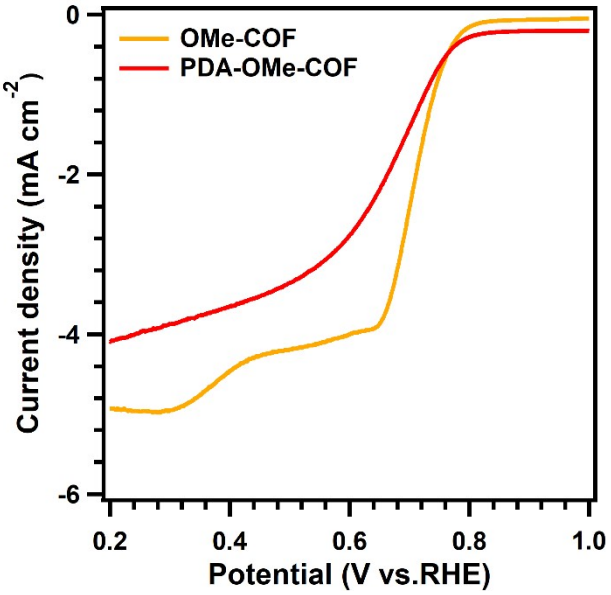

Figure S26. LSV plots at 1600 rpm of OMe-COF, and PDA-OMe-COF in 0.1 M KOH solution

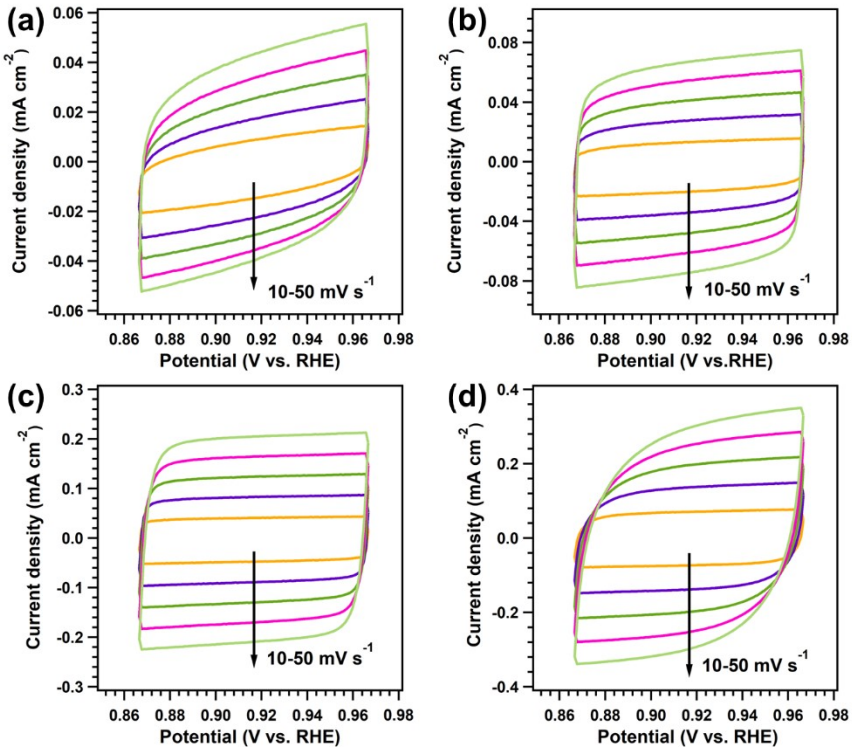

Figure S27. CV curves of (a) H-COF, (b) F-COF, (c) OMe-COF and (d) OH-COF in 0.1 M KOH solution at different scan rates (10, 20, 30, 40 and 50 mV s^{-1}).

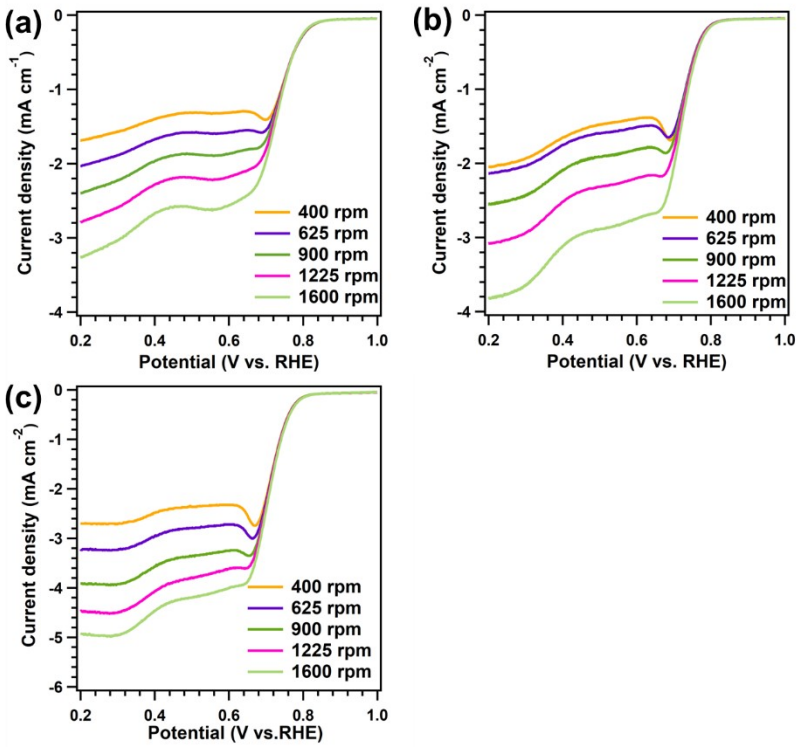

Figure S28. LSV curves of (a) H-COF, (b) F-COFand (c) OMe-COF at various rotation speeds.

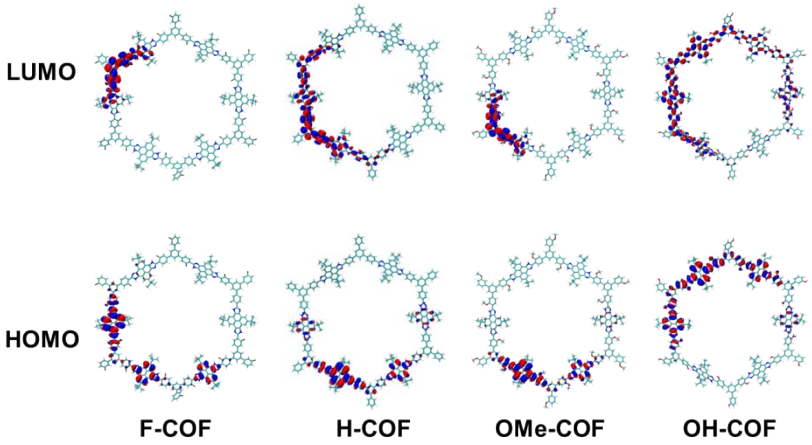

Figure S29. The Kohn-Sham LUMOs and HOMOs of OH-COF, F-COF, H-COF and OMe-COF.

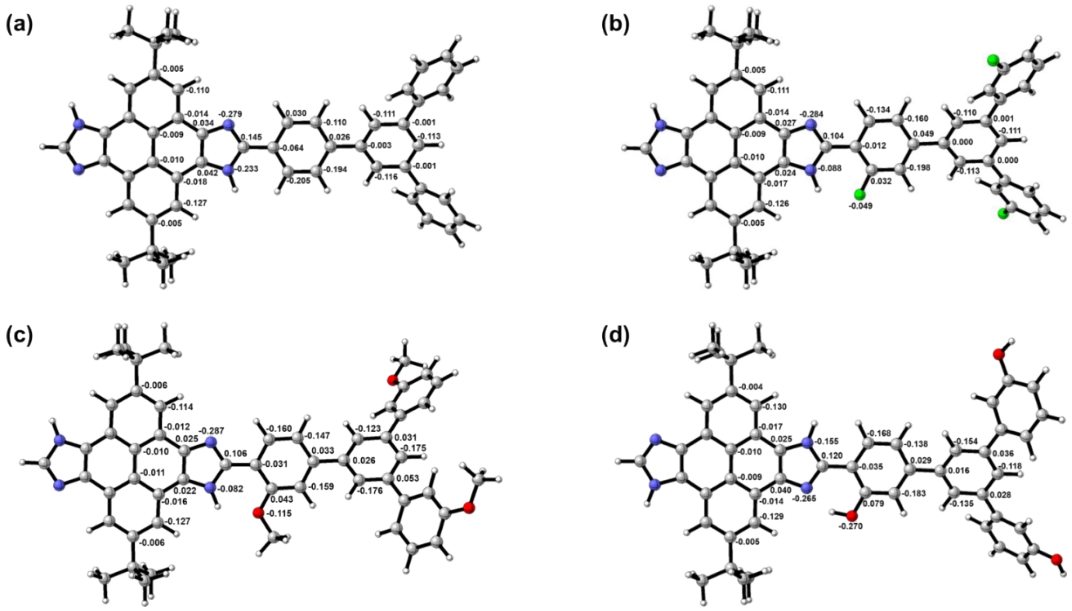

Figure S30. The Hirshfeld atomic charges on main atoms of (a) H-COF, (b) F-COF, (c) OMe-COF and (d) OH-COF. The grey, white, red, blue and green represent carbon, hydrogen, oxygen, nitrogen and fluorine atoms, respectively.

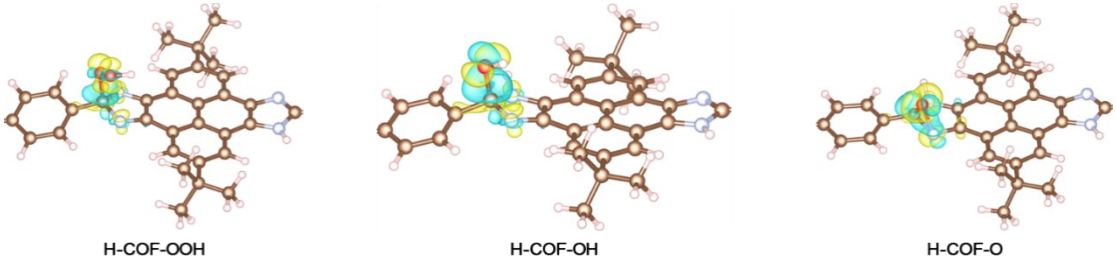

Figure S31. The charge distribution of the adsorption of different ORR intermediates by H-COF. The reddish brown, blue-grey and white spheres represent C, N and H atoms, respectively.

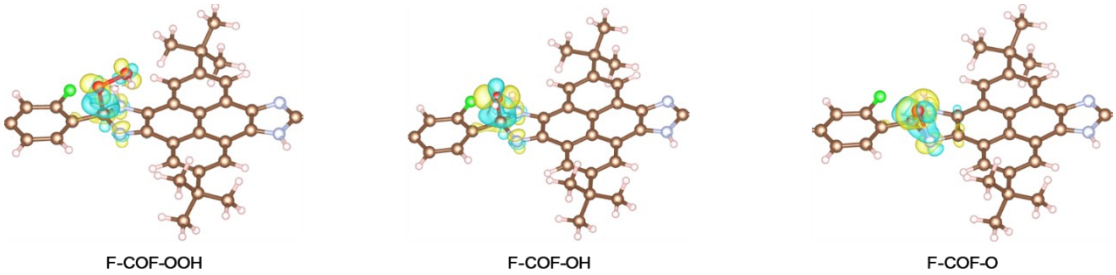

Figure S32. The charge distribution of the adsorption of different ORR intermediates by F-COF. The reddish brown, blue-grey, white and green spheres represent C, N, H and F atoms, respectively.

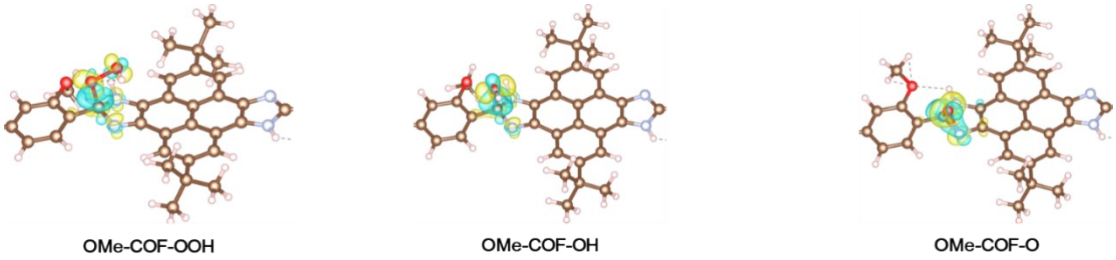

Figure S33. The charge distribution of the adsorption of different ORR intermediates by OMe-COF. The reddish brown, blue-grey, white and red spheres represent C, N, H and O atoms, respectively.

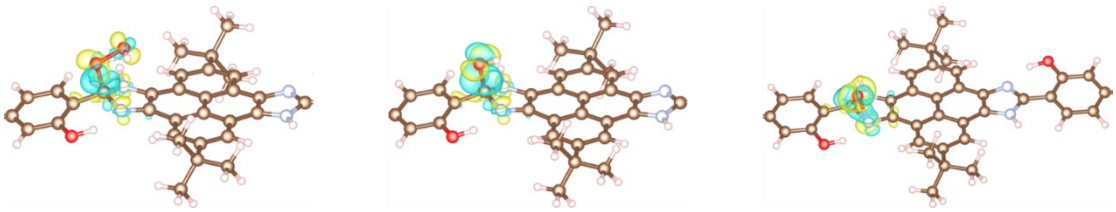

Figure S34. The charge distribution of the adsorption of different ORR intermediates by OH-COF. The reddish brown, blue-grey, white and red spheres represent C, N, H and O atoms, respectively.

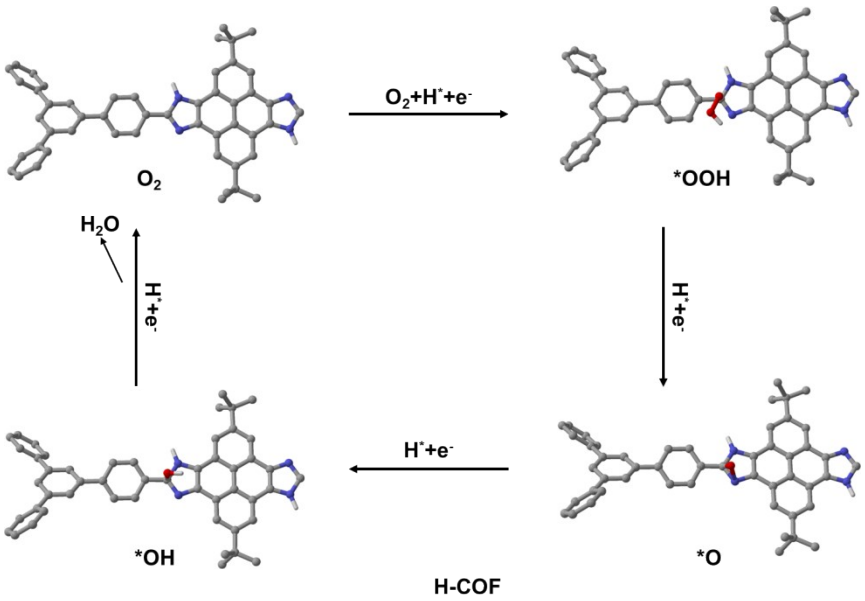

Figure S35. The ORR process structure diagram of H-COF. The grey, white, blue and red spheres represent C, H, N and O atoms, respectively.

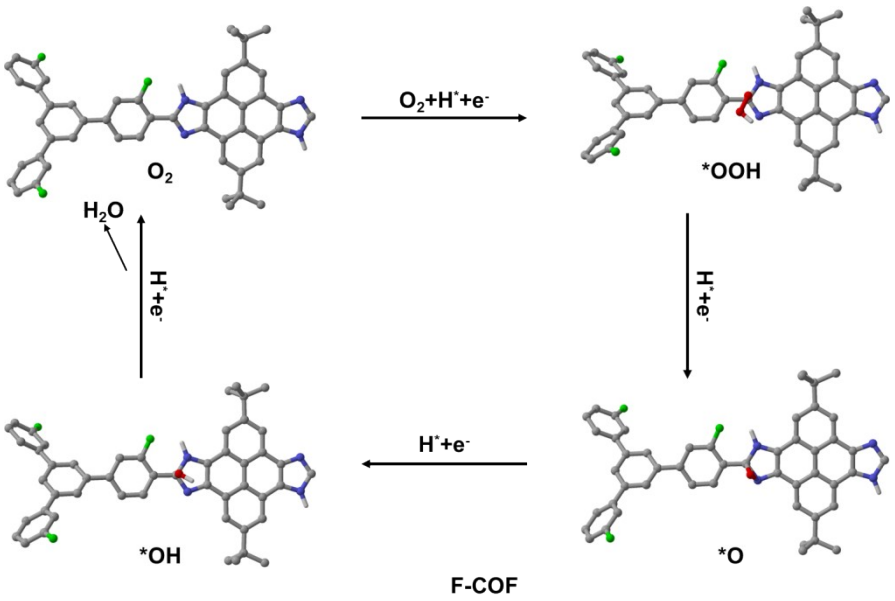

Figure S36. The ORR process structure diagram of F-COF. The grey, white, blue, green and red spheres represent C, H, N, F and O atoms, respectively.

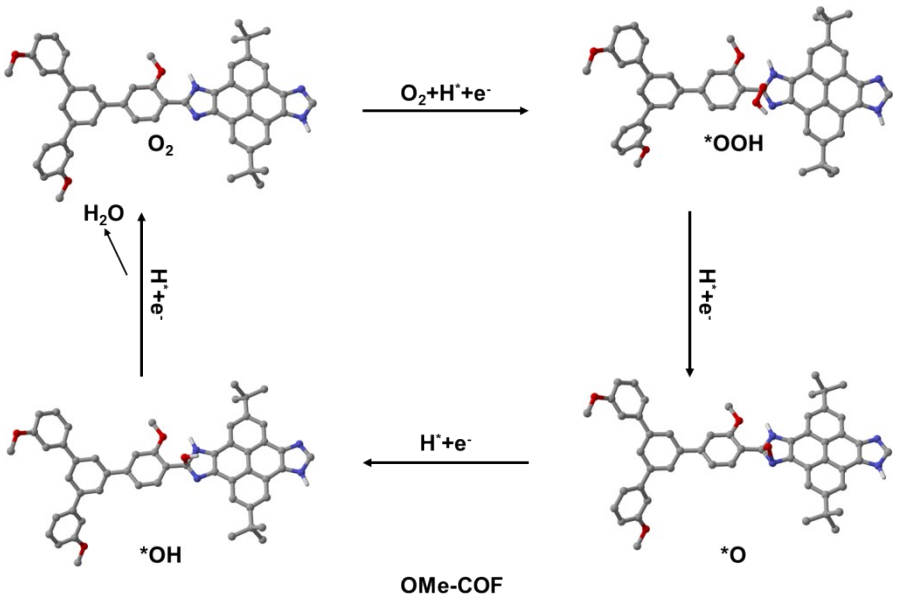

Figure S37. The ORR process structure diagram of OMe-COF. The grey, white, blue and red spheres represent C, H, N and O atoms, respectively.

Section 3. Supporting Tables

Table S1. Comparative ORR activity table with recently reported benchmark COF catalysts.

Catalysts	With/without electronic effect groups	E_{onset} (V) vs.RHE	$E_{1/2}$ (V) vs.RHE	Ref.
COF-β	Without	0.88	0.76	S8
JUC-528	Without	0.83	0.70	S9
Imide-COF	Without	0.79	0.62	S10
Azine-COF	Without	0.84	0.74	
Oxazole-COF	Without	0.85	0.75	
Azo-COF	Without	0.88	0.68	S11
BUCT-COF-11	Without	0.84	0.72	S12
PTh-COF	Without	0.85	0.75	S13
DAF-COF	Without	0.89	0.74	S14
NDI-COF	Without	0.85	0.70	S15
DAPT-TFP-COF	Without	0.79	0.69	S16
TAPA-NDI-COF	Without	0.70	0.61	S17
OH-COF	With	0.89	0.80	**This work**

Section 4. References

[S1] J. Tao, J. P. Perdew, V. N. Staroverov, G. E. Scuseria, *Phys. Rev. Lett.*, 2003, **91**,146401.

[S2] S. Grimme, S. Ehrlich, L. Goerigk, *J. Comp. Chem.*, 2011, **32**,1456-1465.

[S3] F. Neese, *Mol. Sci*., 2018, **8**, e1327.

[S4] CP2K website, http://www.cp2k.org/.

[S5] J. P. Perdew, K. Burke, M. Ernzerhof, *Phys. Rev. Lett.*, 1996, **78**,3865-3868.

[S6] T. Lu, Q. Chen, A, Shermo, *Comput. Theor. Chem*., 2021, **1200**, 113249.

[S7] T. Lu, Chen, F. Multiwfn, *J. Comput. Chem.*, 2012, **33**,580-592.

[S8] Q. Wang, C. Wang, K. Zheng, B. Wang, Z. Wang, C. Zhang, X. Long, *Angew. Chem. Int. Ed.*, 2024, **63**, No. e202320037.

[S9] D. Li, C. Li, L. Zhang, H. Li, L. Zhu, D. Yang, Q. Fang, S. Qiu, X. Yao *J. Am. Chem. Soc.*, 2020**, 142,** 8104-8108.

[S10] X. Li, S. Yang, M. Liu, X. Yang, Q. Xu, G. Zeng, Z. Jian *Angew. Chem. Int. Ed.*, 2023, **62**, No. e202304356.

[S11] M. Martínez-Fernández, E. Martínez-Periñán, S. Royuela, J. I. Martínez, F. Zamora, E. Lorenzo, J. L. Segura, *Appl. Mater.*, 2022, **26**, No. 101384.

[S12] R. Bao, A. Xiang, Z. Qiao, Y. Yang, Y. Zhang, D. Cao, S. Wang, *Angew. Chem. Int. Ed.*, 2023, **62**, No. e202216751.

[S13] Z. Chen, P. Fang, X. Zou, Z. Shi, J. Zhang, Z. Sun, S. Guo, F. Yan, *Small*, 2024, **20**, 2401880.

[S14] Z. You, B. Wang, Z. Zhao, Q. Zhang, W. Song, C. Zhang, X. Long, Y. Xia, *Adv. Mater.*, 2023, **35**, No. 2209129.

[S15] S. Royuela, E. Martínez-Periñán, M. P. Arrieta, J. I. Martínez, M. M. Ramos, F. Zamora, E. Lorenzo, J. L. Seguraet, *Chem. Comm.*, 2020, **56**, 1267-1270.

[S16] P. García-Arroyo, E. Martínez-Periñán, J. J. Cabrera-Trujillo, E. Salagre, E. G. Michel, J. I. Martínez, E. Lorenzo, J. L. Segura, *Nano Res.*, 2022, **15**, 3907-3912.

[S17] M. Martínez-Fernández, E. Martínez-Periñán, S. Royuela, J. I. Martínez, F. Zamora, E. Lorenzo, J. L. Segura, *Appl. Mater.*, 2022, **26**, No. 101384.